JOIV : Int. J. Inform. Visualization, 7(1) - March 2023 15-21

INTERNATIONAL JOURNAL ON INFORMATICS VISUALIZATION

journal homepage : www.joiv.org/index.php/joiv

Solar Powered Vibration Propagation Analysis System using nRF24l01 based WSN and FRBR

Wirarama Wedashwara [a,*], Made Sutha Yadnya [b], I Wayan Sudiarta [c], I Wayan Agus Arimbawa [d], Tatang Mulyana [e]

[a] *Deparment of Informatics Engineering, University of Mataram, Mataram, Indonesia*
[b] *Department of Electrical Engineering, University of Mataram, Mataram, Indonesia*
[c] *Department of Physics, University of Mataram, Mataram, Indonesia*
[d] *Department of Technology Management, Economics, and Policy, Seoul National University, Seoul, Republic of Korea*
[e] *Department of Information System, Telkom University, Bandung, Indonesia*
Corresponding author: [*]wirarama@unram.ac.id

***Abstract*— Prevention of the effects caused by natural disasters such as earthquakes and landslides requires analysis of vibration propagation. In outdoor applications, internet sources such as WIFI are not always available, so it requires alternative data communications such as nRF24l01. The system also requires a portable power source such as solar power. This research aims to develop a vibration propagation analysis system based on the nRF24l01 wireless sensor network and solar power by implementing the fuzzy rule-based regression (FRBR) algorithm. The system consists of two piezoelectric and nrf24l01 vibration sensors. The system also uses a third node equipped with temperature and soil moisture sensors, air temperature and humidity, and light intensity as environmental variables. The evaluation results show the Quality of Services (QoS) results with a throughput of 99.564%, PDR 99.675%, and a delay of 0.0073s. The Fuzzy Association Rule (FAR) extraction results yield nine rules with average support of 0.319 and confidence of 1 for vibration propagation. The availability of solar power was evaluated with an average current value of 0.250A and a voltage of 3.266V. The results of FRBR are based on the propagation of the vibration that propagated and produced a mean square error (MSE) of 0.141 and a mean absolute error (MAE) of 0.165. The correlation matrix and FAR results show that only soil moisture has a major effect on the magnitude and duration of propagation. However, other variables can regress soil moisture with MSE 0.232 and MAE 0.287.**

***Keywords*— Internet of Things; fuzzy association rule mining; wireless sensor networks.**

Manuscript received 22 Mar. 2022; revised 29 Aug. 2022; accepted 25 Dec. 2022. Date of publication 31 Mar. 2023.

I. INTRODUCTION

Prevention of the effects caused by natural disasters such as earthquakes and landslides requires analysis of vibration propagation [1]. Vibration measurements can be measured using a vibration sensor such as a piezoelectric sensor [2]. The propagation can be determined by comparing the source and destination vibrations [3], [4]. In outdoor applications, internet sources such as WIFI are not always available [5], so alternative data communications such as nRF24l01 are needed [6]–[8]. The system also requires a portable power source such as solar power [9], [10]. Vibration measurements can be measured using a vibration sensor such as a piezoelectric sensor. Its propagation can be determined by comparing the source and propagation vibrations so that the node can be installed anywhere if it is within the range of nRF24l01 and there is sunlight for charging the battery.

This study aims to develop a vibration propagation analysis system based on the nRF24l01 wireless sensor network, solar-powered, and data analysis using a fuzzy rule-based regression (FRBR) algorithm. The system consists of two piezoelectric and nrf24l01 vibration sensors. The system also uses a third node equipped with temperature and soil moisture sensors, air temperature and humidity, and light intensity as environmental variables.

System evaluation from the functional side includes analysis of the Internet of Things (IoT)[11], Quality of Service (QoS) [12] , and solar power availability. The main evaluation of the research in testing the algorithm includes a description of the data collected from the IoT nodes, the correlation matrix of the data collected from the IoT nodes

and 6 test schemes and rules, and an analysis of the regression results. The system will be tested by performing vibrations on the source node and comparing it with the vibrations that propagate to the second node. The tests were carried out under various weather conditions, both air and soil conditions. The vibration simulation is only done manually using the pounding of the feet from various heights and human body weight. The test was carried out for two days by comparing various vibrations, temperature conditions, and soil moisture.

The research focuses on testing IoT devices and regression results on the magnitude of the vibration that propagates. The study did not specifically discuss environmental aspects such as soil conditions and creating vibrations [13]. The nRF24l01 network topology used is a star topology with data nodes one and two containing piezoelectric sensors sending data to node three containing environmental sensors.

Research related to earthquake detection using IoT has been carried out previously to develop a low-cost notification system [14], early warning using a smart meter [15] , and data transmission using MQTT [16]. All three studies focused on developing a single device and did not detect vibration propagation. This study uses two devices to detect propagation and environmental conditions' influence on propagation's magnitude.

Research related to the use of piezoelectric vibration sensors and nRF24l01 has been carried out for Medical Electromyography [17] and rolling bearings [18]. Both studies focus on applications in medical devices. The proposed research focuses on vibration propagation in the soil. Vibration propagation in the soil has differences based on soil conditions influenced by the environment.

Research on the development of an algorithm to detect earthquakes has been carried out using the Gaussian process for post-earthquake building conditions [19], sequential regression-based predictive mean matching to fill in the missing data due to data communication disturbances [20], and magnitude relation regression for Sudan territory [21].

II. Materials and Method

Figure 1 shows an overview of the system. The system consists of two vibration nodes and an environment node. The environment node consists of ambient temperature and humidity sensors, light intensity sensors, and soil temperature sensors. The environment node serves to determine the relationship between environmental conditions and the conditions on the vibration node. Air temperature, humidity, light intensity, and soil temperature were chosen because they affect soil moisture.

The two vibration nodes consist of a vibration sensor and a soil humidity sensor. The main function of the vibration node is to measure the vibration propagation from source to destination. The vibration sensor compares the ground vibration at the source to the destination not only once but the duration until the vibration subsides. Both vibration nodes are equipped with soil humidity to determine the effect of soil moisture on vibration propagation. Soil moisture was chosen because it is a variable that the sensor can measure. Soil moisture is also a test scenario by comparing different soil moisture conditions from source to destination nodes—for example, the wet source node and dry destination or both wet.

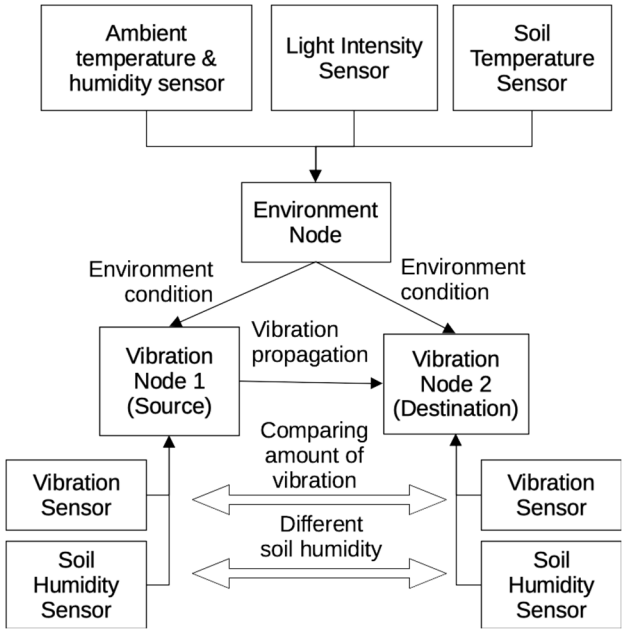

Fig. 1 General View of The System

Figure 2 shows a flowchart of the system. The system starts with the preparation of IoT devices, land, and water. Then, testing with different soil moisture scenarios was carried out at the source and destination nodes. This is done under different environmental conditions to test changes in soil moisture that will cause differences in vibration intensity between the source and destination nodes.

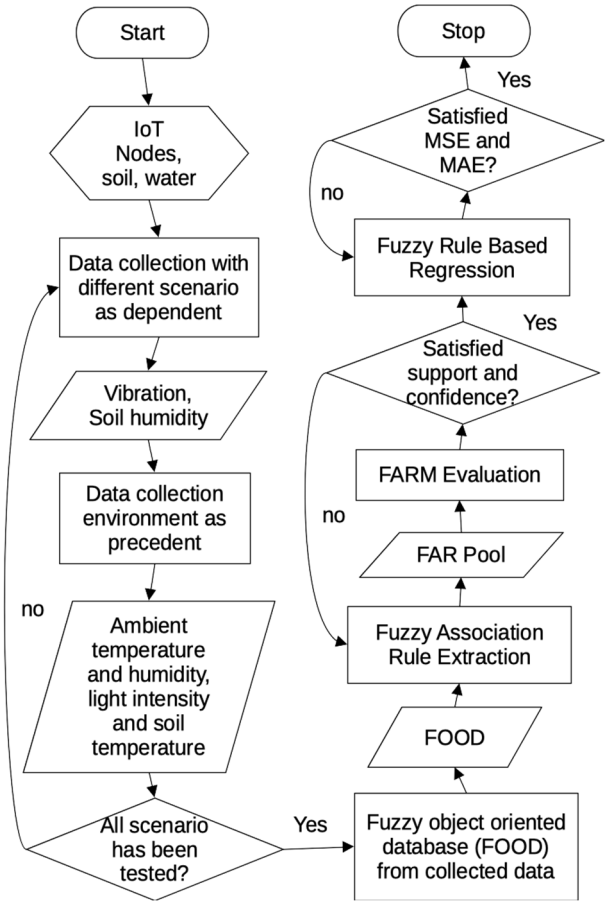

Fig. 2 Flowchart of the system

Vibration testing is carried out by manual stomping and a machine drill on the ground. Footsteps are used to simulate instantaneous vibrations, while machine drills simulate continuous vibrations. The test is carried out until all vibration scenarios are periodically carried out at different soil moisture and environmental conditions. The collected data is processed into a Fuzzy Object-Oriented Database (FOOD) developed in previous research [22]. FOOD is then assembled into a Fuzzy Association Rule (FAR) using a FAR extractor. Furthermore, FARM evaluation is carried out, namely support and confidence. The extraction process is carried out until the support and confidence threshold values are reached.

Fuzzy Rule-Based Regression (FRBR) used in this study uses an algorithm that has been developed by the previous author [23]. The rule-based regression process is carried out with environmental conditions as precedent and vibration propagation dependent. Regression in this study was carried out in two stages. The first regression is the influence of the environment on soil moisture. The second and major regression is vibration propagation based on soil moisture conditions, so this research is expected to estimate the level of vibration propagation based on environmental patterns that affect the soil.

III. Results and Discussion

A. *Developed IoT Nodes*

Figure 3 shows the electrical schematic of the vibration node. The components consist of Arduino nano as a microcontroller and nRF24L01 as a data communication module. nRF24L01 is connected to 3.3v and other digital inputs. nRF24L01 on both vibration nodes only sends data to the environment node, which will upload data to the internet via the GSM module.

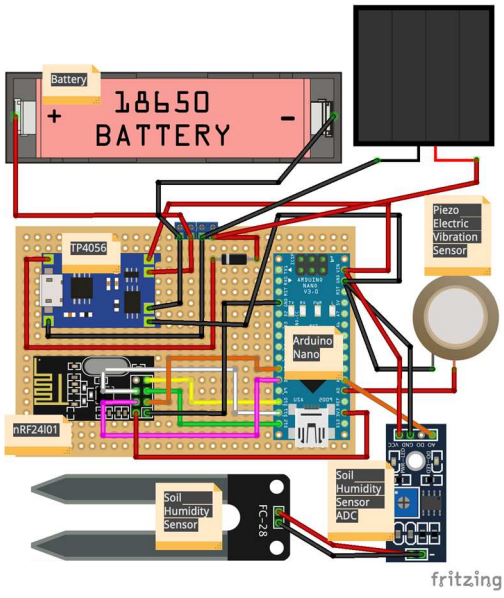

Fig. 3 Electrical Scheme of The Vibration Node

The first input is a piezoelectric vibration sensor to measure vibration. The piezoelectric vibration sensor is connected via analogue 0 as input, power supply, and ground. The second input is a soil moisture sensor connected via an analog to digital converter module to measure soil moisture. The soil moisture sensor is connected to the Arduino nano via analog one and 5v and the power supply.

The vibration node is also connected to the TP4056 charging module to connect a small solar panel and a 18650 battery with a capacity of 1.2 Ah and a voltage of 3.7v. The solar power source allows the system to run completely wirelessly for both the power source and data communication media.

Figure 4 shows the electrical schematic of the environment node. The environment node functions to collect data related to the environment and connects to the internet via the GSM module SIM800L. Internet access via GSM allows the system to run without depending on the availability of WIFI to be applied in outdoor applications. SIM800L requires a step-up module to increase the voltage from 3.7v to 4.2v required in its operation.

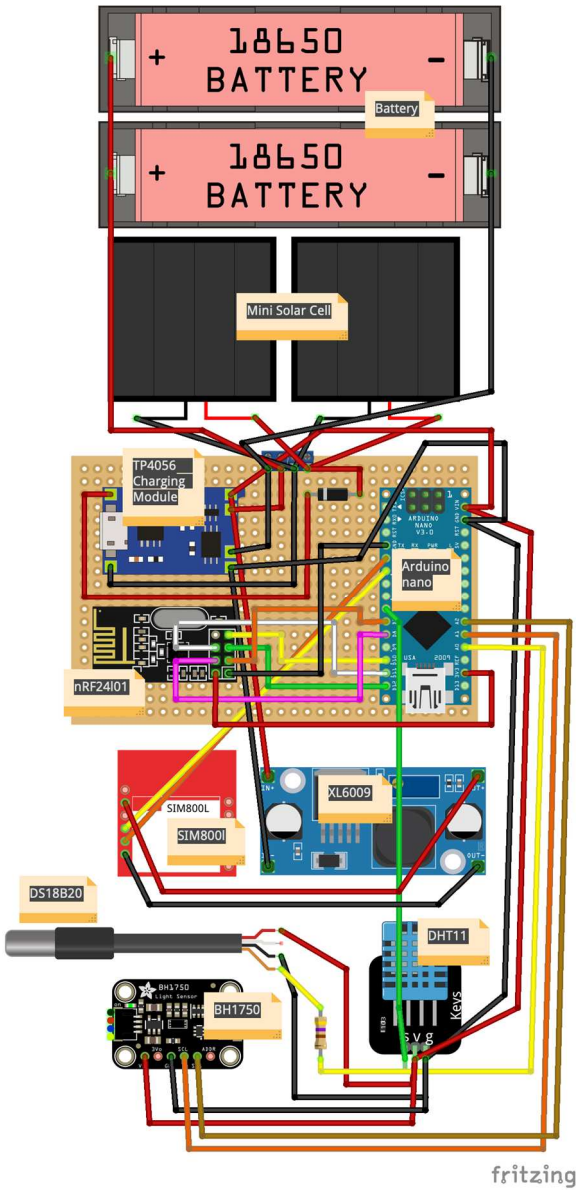

Fig. 4 Electrical Scheme of The Environment Node

The environment node is also connected to the nRF24L01 to receive data from the vibration node and upload it to the internet via the GSM module. NRF24L01 on the environment node waits for data from the two vibration nodes and uploads

it together with data from the three sensors on the environment node to the internet in the form of one line of text and is read by a script on the data storage server. The input is BH1750 which is the light intensity sensor, DHT11 is the temperature and humidity of the air, and DS18B20 is the soil temperature sensor. BH1750 and DS18B20 are connected to the analogue input with a voltage of 5v. DHT11 is connected to a digital input with a voltage of 5v. The three sensors are connected to a 5v voltage to be paralleled with a single power source.

The TP4056 is connected to two solar panels and two 18650 batteries in parallel to maximize capacity. The solar panels arranged in parallel allow a current supply of up to 2A. The 18650 batteries in parallel allows a capacity of up to 2.4 Ah. The environmental node's heavy electrical load is expected to continue operating while uploading data.

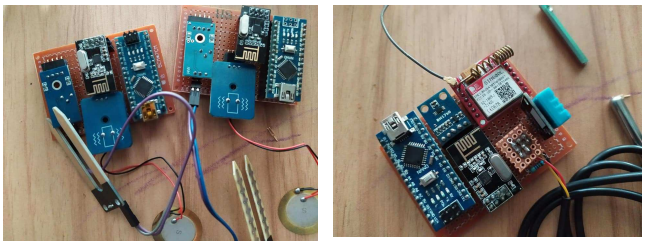

(a) node 1 and 2 (b) node 3

Fig. 5 Actual view of IoT nodes

Figure (a) of 5 shows a pair of vibration nodes that will serve as the source and destination of vibration propagation. The electrical circuit is connected by a 30 AWG cable soldered on a 5×7cm single layer PCB. Each component is connected to a female header so that it can be replaced easily if there is component damage. The power source is mounted on a different PCB and mounted on the enclosure box. Figure (b) of 5 shows the result of the environment node, which functions to measure the environmental condition sensor input and uploads data to the internet via the GSM module. The environment node circuit relates to a 30 AWG cable soldered to a 5×7cm single layer PCB. The environment node is placed in a larger enclosure due to the placement of two batteries and solar panels.

B. Evaluation of the QoS

Table 1 shows the refresh rate and sensor packets connected to each IoT Node. Nodes 1 and 2 are vibration nodes connected to a piezoelectric vibration sensor with a refresh rate of 200ms and a soil moisture sensor with 500ms. So, a total of two nodes generates twice 700ms, which is 1400ms. The piezoelectric vibration sensor measures vibrations with resistance between 0 to 1023. The greater the resistance value, the greater the resistance value. The soil moisture sensor also has a humidity value based on resistance from 0 to 950. Resistance values 0~300 indicate dry soil, 300~700 indicate moistness, and 700~950 indicate conditions in water [24]. The piezoelectric vibration sensor uses 4 bytes, and the soil moisture sensor uses 3 bytes from the data packet. So, nodes 1 and 2 use a total of twice 7 bytes which is 14 bytes.

The environment node is connected to a light intensity sensor, DHT11 and a soil temperature sensor, each with a 1000ms refresh rate. So, the total has a 3s refresh rate. The light intensity sensor has a value from 0 to 65535 Lux. The higher the Lux value, the brighter it is. DHT11 produces temperature values between 00.00 to 50.00 Celsius degree and humidity of 100%. The DS18B20 produces temperature values from -55 to 125 Celsius degree. The total data packet used is 31 bytes with a 4400ms refresh rate. An example of the format of the packet being sent appears at the very bottom of the character column. The type of data sent is char with a fixed size of 32. So, to save data packets and ease programming work on the microcontroller side, there is no separator, and the value of each variable is called through an index array.

TABLE I
REFRESH RATE AND PACKET SIZE OF EACH NODE

N	Sensor	RR (ms)	Characters	PS (byte)
1	Piezo Electric Vibration Sensor (Ω)	200	0000~1023	4
	Soil Moisture (Ω)	500	000~950	3
2	Piezo Electric Vibration Sensor (Ω)	200	0000~1023	4
	Soil Moisture (Ω)	500	000~950	3
3	Light Intensity (Lux)	1000	00001~65535	5
	DHT11 (°C and %)	1000	00.00000~50.00100	8
	DS18B20 (°C)	1000	-055~+125	4
		4400	0001001000100100000101.01001+001	31

Table 2 shows the results of the QoS evaluation of the star topology used in this study. The use of star topology has been investigated more efficiently for distances centered in previous studies [25]. Each node is separated by 400m, 40% of the maximum distance of nRF24l01. So that the closer distance results in higher throughput (99.564%) and PDR (99.675%) values than previous studies. However, the delay value is higher (0.0073ms) because the data packets sent are bigger.

TABLE II
QOS OF STAR TOPOLOGY

Node	Throughput (%)	PDR (%)	Delay (ms)
1	99.672	99.865	0.003
2	99.673	99.863	0.006
3	99.347	99.298	0.013
	99.564	99.675	0.007

Table 3 shows the availability of solar power for one day to ensure the system can run fully in sunny weather conditions. The evaluation also ensures the relationship between data communication quality and energy availability. Light intensity was measured using BH1750, and the temperature was measured using DHT11. Current is measured using ACS712, and voltage is measured using a 32V DC Voltage sensor using a tool developed in previous research [26].

TABLE III
EVALUATION OF SOLAR AVAILABILITY

T(h)	L (lux)	Temp °C	Solar Cells C(A)	Solar Cells V(V)	Batteries C(A)	Batteries V(V)	Thr (%)	PDR (%)	Dly (s)
08-11	14678	28.33	0.543	4.219	0.231	3.713	99.923	99.312	0.001
11-16	45021	31.82	0.381	5.201	0.223	3.614	99.321	99.613	0.002
16-18	14987	30.22	0.286	4.201	0.291	3.351	99.872	99.312	0.002
18-20	5346	28.34	0.156	0.142	0.248	3.113	99.892	98.243	0.012
20-05	123	27.68	0	0	0.234	2.968	99.891	94.221	0.023
05-08	12983	28.26	0.356	4.354	0.242	2.891	99.888	95.399	0.014
08-11	15012	28.16	0.657	4.134	0.274	3.143	99.634	97.692	0.012
11-16	45021	29.31	0.478	5.456	0.254	3.332	99.242	99.376	0.013
	19146	29.01	0.357	3.46	0.250	3.266	99.708	97.896	0.010

Like the pattern in previous research [26], the energy produced by solar panels decreases when the light intensity is reduced and the air temperature is too high. However, it can still be recharged the next day when light conditions improve. Throughput is not affected, and PDR and delay have little effect when battery voltage drops. Because it uses a step-up module, the voltage received by the sensor can still be held stable.

Data translation is done by fuzzy rule-based clustering (FRBC) [27]. The data collected for one week in the cluster is divided into high and low irrigation water flows. Watering is done without delay, which is set on the programming manually. Watering is carried out if the soil moisture is less than 100Ω and stops when it reaches 500Ω. The research focuses on prototyping tools, so calibration has not been carried out for ideal irrigation for certain crops. The membership function used is a gaussian asymmetric, which involves the lower standard deviation(σ1), upper(σ2) and means(μ[19], [28].

C. Evaluation of Collected Data

Table 4 shows six scenarios carried out to obtain vibration propagation data. Each scenario (Sk) shows a combination of source vibration magnitude (VS), vibration duration (VD), source soil moisture (SHS), destination soil moisture (SHD) to measure the magnitude of the vibration that propagates to the destination (VD) and its duration (VDD). The scenarios are separated based on three vibration magnitudes and their duration (short and long) so that there are six scenarios. Each scenario is further divided into three types of soil moisture variations: dry, only wet, and equally wet sources, resulting in 18 sub scenarios. Each of the 18 scenarios was tested 20 times for a total of 360 tests.

Scenarios 1 and 2 show small vibrations. Scenario 1 for a short duration reduces vibration to the destination by 15.972% for equally dry conditions, 23.288% for the wet side and 19.205% for both wet conditions. The vibration duration did not differ much for the three conditions of soil moisture, which was reduced by an average of up to 26.407%. Scenario 2, with small vibrations and long duration, reduced the average vibration that propagates to 40.071%. On the other hand, the wet humidity condition still produces the highest value, which is 44.371%. The vibration duration lasts greater than an average of 99.214%.

Scenarios 3 and 4 show the simulation results of the moderate vibrations. Scenario 3 for a short duration resulted in vibration propagation with an average of 47.971%, which increased 28.483% from scenario 1. The duration did not increase; an average of 30.824% only increased by 4.416% from scenario 1. Scenario 4 for long-duration resulted in an average reduction vibration of 58.654%, which is an increase of 18.584% from scenario 2. The duration is smaller than scenario 2 with an average of 87.111%, reduced by 12.103%.

Scenarios 5 and 6 show the simulation result of the big vibrations. Scenario 5 for a short duration produces vibration propagation with an average of 63.651%, an increase of 15.680% from scenario 3. The vibration duration produces an average of 55.551%, increasing by 24.727% from scenario 3. Scenario 6 for a long duration produces the highest average propagation, namely 80.045% increased by 21.391% from scenario 4. The propagation duration to last up to an average of 99.625% increased by 12.513% from scenario four and only 0.411% difference from scenario 2.

TABLE IV
COLLECTED DATA BASED ON EVALUATION SCENARIO

s	V_S (Ω)	VD_S (ms)	SH_S (Ω)	SH_D (Ω)	V_D (Ω)	VD_D (ms)
1	144	1623	201	213	23	456
	146	1982	678	211	34	502
	151	1973	687	672	29	509
2	153	57256	212	221	56	56789
	151	57829	692	232	67	57126
	158	58192	688	689	62	58002
3	453	1926	208	203	172	620
	461	2014	682	205	273	612
	458	2141	689	682	214	640
4	437	58201	208	202	254	50278
	442	58312	698	223	268	51021
	451	58321	691	682	258	51002
5	834	2237	204	207	535	1283
	842	2415	697	212	536	1289
	852	2321	676	682	538	1298
6	858	57629	206	207	678	58920
	861	58267	687	208	698	58932
	852	58301	686	689	682	58289

Table 5 shows the correlation matrix between the variables tested in the study. The variables consist of SH (soil humidity), ST (Soil Temperature), L (Light Intensity), AT(Ambient Temperature) and AH(Ambient Humidity). Meanwhile, V_S, V_D, VD_S, VD_D are following the explanation in table 4. The green column shows the correlation above 0.5. V_S and V_D have the highest correlation, namely 0.987, followed by VD_S and VD_D with a value of 0.986. AH also has a high correlation with AT.

TABLE V
CORRELATION MATRIX

	SH	ST	L	AT	AH	V_S	V_D	VD_S	VD_D
SH	1	0.456	0.236	0.237	0.345	0.345	0.656	0.357	0.768
ST	0.456	1	0.145	0.456	0.245	0.125	0.104	0.102	0.101
L	0.236	0.145	1	0.342	0.265	-0.367	-0.325	-0.289	-0.223
AT	0.237	0.456	0.342	1	0.563	-0.365	-0.356	-0.345	-0.323
AH	0.345	0.245	0.265	0.563	1	-0.267	-0.178	-0.189	-0.188
V_S	0.345	0.125	-0.367	-0.365	-0.267	1	0.987	-0.345	-0.456
V_D	0.656	0.104	-0.325	-0.356	-0.178	0.987	1	-0.537	-0.453
VD_S	0.357	0.102	-0.289	-0.345	-0.189	-0.345	-0.537	1	0.986
VD_D	0.768	0.101	-0.223	-0.323	-0.188	-0.456	-0.453	0.986	1

The red column shows a low correlation below 0.2. V_S, V_D, VD_S, VD_D are the values in the scenario so that they have a low correlation with other variables except for SH, 0.656 with VD_D and 0.768 with VD_D. L also has a low correlation with SH. The yellow column indicates an intermediate correlation between 0.2 and 0.5. Environmental variables have a moderate correlation with each other. SH in the data obtained in this study did not show a high correlation with ST.

D. Evaluation of FARM

Table 6 shows the results of the FAR and its evaluation, namely support and confidence. Table 6 shows the rules sorted by the size of the support. Rules 1 to 3 show the precedent relation V_S and VD_S to the dependent V_D and VD_D, with the numbers after that showing the quantities ordered by the fuzzy membership function [29], [30]. The support value reaches an average of 0.319, and confidence reaches a value of 1; namely, the absolute precedent and dependent

relationship occur. Rules 4 to 6 show a similar precedent relationship with the addition of SH, which in table 5 shows a high correlation. However, the addition of SH lowers support to an average of 0.270 and a confidence value of 0.818.

Rules 7 to 9 show the environmental conditions ST, AH, AT, and L as precedent and SH as a dependent. This relationship produces average support of 0.127 and confidence of 0.803. Rule 9 is the longest precedent, but the support is only 0.101, with better confidence than rules 7 and 8, 0.893. Rule 9 is the only rule involving L, which has the lowest correlation to SH (table 5). Overall, FAR results show an average of 0.239 support and 0.874 confidence.

TABLE VI
EXTRACTED RULES AND EVALUATION

Index	Precedent	Dependent	Support	Conf
1	$\{V_{S1},VD_{S1}\}$	$\{VD_{1},,VD_{D1}\}$	0.324	1
2	$\{V_{S2},VD_{S2}\}$	$\{VD_{3},,VD_{D3}\}$	0.316	1
3	$\{V_{S3},VD_{S3}\}$	$\{VD_{3},,VD_{D3}\}$	0.318	1
4	$\{V_{S3},VD_{S3},SH_{2}\}$	$\{VD_{3},,VD_{D3}\}$	0.276	0.822
5	$\{V_{S2},VD_{S2},SH_{2}\}$	$\{VD_{2},,VD_{D2}\}$	0.271	0.819
6	$\{V_{S1},VD_{S1},SH_{2}\}$	$\{VD_{1},,VD_{D1}\}$	0.262	0.813
7	$\{ST_{1},AH_{1}\}$	$\{SH_{1}\}$	0.148	0.725
8	$\{ST_{2},AH_{2},AT_{2}\}$	$\{SH_{2}\}$	0.132	0.792
9	$\{ST_{2},AH_{2},AT_{2},L_{2}\}$	$\{SH_{2}\}$	0.101	0.893
Average			0.239	0.874

Table 7 shows the results of the regression using FRBR. The test is divided into five conditions based on the regression rules (Table 6). Regression was tested using mean square error (MSE) and mean absolute error (MAE) [31], [32]. Conditions 1 and 3 show the same results, namely MSE 0.141 and MAE 0.165. This is because FRBR will choose the rule with the highest support and confidence, so rules 1 to 3 are selected. Condition four supports this, which has an increasing error with MSE 0.362 and MAE 0.387 because it does not involve rules 1 to 3.

TABLE VII
REGRESSION RESULTS OF FRBR

i	Rules	MSE	MAE
1	All	0.141	0.165
2	1~3	0.141	0.165
3	1~6	0.141	0.165
4	4~6	0.362	0.387
5	7~8	0.232	0.287

The correlation matrix and FAR results show that only soil moisture has a major effect on the magnitude and duration of propagation. However, other variables can regress the soil moisture as indicated by condition 5 with MSE 0.232 and MAE 0.287. This additional feature can predict vibration conditions if certain weather conditions persist.

IV. CONCLUSION

Research has developed a solar-powered nRF24L01-based vibration propagation analysis system with regression implementation using FRBR. The evaluation results show the Quality of Services (QoS) results with a throughput of 99.564%, PDR 99.675%, and a delay of 0.0073s. The Fuzzy Association Rule (FAR) extraction results yield nine rules with average support of 0.319 and confidence of 1 for vibration propagation. The availability of solar power has been tested with an average current value of 0.250A and a voltage of 3.266V. The results of FRBR were carried out on the magnitude of the vibration that propagated and produced a mean square error (MSE) of 0.141 and a mean absolute error (MAE) of 0.165. The correlation matrix and FAR results show that only soil moisture has a major effect on the magnitude and duration of propagation. However, other variables can regress soil moisture with MSE 0.232 and MAE 0.287. As an additional evaluation in the future, an analysis will be carried out using other variables such as the type of soil and the placement of the vibration sensor under the ground.

REFERENCES

[1] W. Hu, C. Zhang, and Z. Deng, "Vibration and elastic wave propagation in spatial flexible damping panel attached to four special springs," Commun Nonlinear Sci Numer Simul, vol. 84, p. 105199, 2020.

[2] M. Santhiya, M. Keerthika, M. Shobana, R. Jegatha, and N. S. J. Joan, "An IOT used piezoelectric sensor used power generation through footsteps," *Mater Today Proc*, vol. 37, pp. 166–169, 2021.

[3] L. Zhang, S. Tan, Z. Wang, Y. Ren, Z. Wang, and J. Yang, "VibLive: A Continuous Liveness Detection for Secure Voice User Interface in IoT Environment," in *Annual Computer Security Applications Conference*, 2020, pp. 884–896.

[4] G. Kreshnadhi, I. K. D. Jaya, B. B. Santoso, W. Wangiyana, and H. Suheri, "Application of manures reduces inorganic fertilizers requirement for maize grown in a sandy soil," in *IOP Conference Series: Earth and Environmental Science*, 2021, vol. 913, no. 1, p. 12001.

[5] N. Chungsawat and P. Siripongwutikorn, "Predicting application performance in LoRa IoT networks," in *Proceedings of the 11th International Conference on Advances in Information Technology*, 2020, pp. 1–7.

[6] A. Karra, B. Kondi, and R. Jayaraman, "Implementation of Wireless Communication to Transfer Temperature and Humidity Monitoring Data using Arduino Uno," in *2020 International Conference on Communication and Signal Processing (ICCSP)*, 2020, pp. 1101–1105.

[7] S. D. Ambadkar and S. S. Nikam, "Cost-Efficiently Monitoring and Controlling of Saline Level with Health Constants Based on NRF Transceiver and GSM," *Technology (Singap World Sci)*, vol. 11, no. 9, pp. 151–159, 2020.

[8] H.-C. Lee and K.-H. Ke, "Monitoring of large-area IoT sensors using a LoRa wireless mesh network system: Design and evaluation," *IEEE Trans Instrum Meas*, vol. 67, no. 9, pp. 2177–2187, 2018.

[9] P. Maharjan *et al.*, "A fully functional universal self-chargeable power module for portable/wearable electronics and self-powered IoT applications," *Adv Energy Mater*, vol. 10, no. 48, p. 2002782, 2020.

[10] D. Sarathkumar, K. Venkateswaran, and A. Vijayalaxmi, "Design and implementation of solar powered hydroponics systems for agriculture plant cultivation," *International Journal of Advanced Science and Technology*, vol. 29, no. 5, 2020.

[11] P. Sivaraman and C. Sharmeela, "IoT-Based Battery Management System for Hybrid Electric Vehicle," *Artificial Intelligent Techniques for Electric and Hybrid Electric Vehicles*, pp. 1–16, 2020.

[12] N. Varyani, Z.-L. Zhang, and D. Dai, "QROUTE: an efficient quality of service (QoS) routing scheme for software-defined overlay networks," *IEEE Access*, vol. 8, pp. 104109–104126, 2020.

[13] F. A. Purnomo, N. M. Yoeseph, S. A. T. Bawono, and R. Hartono, "Development of air temperature and soil moisture monitoring systems with LoRA technology," in *Journal of Physics: Conference Series*, 2021, vol. 1825, no. 1, p. 12029.

[14] J. Won, J. Park, J.-W. Park, and I.-H. Kim, "BLESeis: low-cost IOT sensor for smart earthquake detection and notification," *Sensors*, vol. 20, no. 10, p. 2963, 2020.

[15] A. Taale, C. E. Ventura, and J. Marti, "On the feasibility of IoT-based smart meters for earthquake early warning," *Earthquake Spectra*, p. 8755293020981964, 2021.

[16] Y. Chen, R. Cui, X. Zhu, Y. Zhou, Z. Lin, and M. Liu, "Transmission earthquake waveform using IOT MQTT protocol," *Progress in Geophysics*, vol. 35, no. 4, pp. 1232–1237, 2020.

[17] M. Falah, S. Mohammed, and S. Gharghan, "PZT, EMG, nRF24L01 Energy Harvesting-based Vibration Sensor for Medical Electromyography Device," *International Journal of Electrical and Electronic Engineering \& Telecommunications*, 2020.

[18] L. Zhang, F. Zhang, Z. Qin, Q. Han, T. Wang, and F. Chu, "Piezoelectric energy harvester for rolling bearings with capability of self-powered condition monitoring," *Energy*, vol. 238, p. 121770, 2022.
[19] M. Sheibani and G. Ou, "The development of Gaussian process regression for effective regional post-earthquake building damage inference," *Computer-Aided Civil and Infrastructure Engineering*, vol. 36, no. 3, pp. 264–288, 2021.
[20] H. Luo and S. G. Paal, "Advancing post-earthquake structural evaluations via sequential regression-based predictive mean matching for enhanced forecasting in the context of missing data," *Advanced Engineering Informatics*, vol. 47, p. 101202, 2021.
[21] M. Ezzelarab, K. Y. Ibrahim, and A. A. Mohamed, "Earthquake magnitude regression relationships for Sudan territory," *Journal of African Earth Sciences*, vol. 183, p. 104326, 2021.
[22] W. Wedashwara, S. Mabu, M. Obayashi, and T. Kuremoto, "Evolutionary Rule Based Clustering for Making Fuzzy Object Oriented Database Models," in *Advanced Applied Informatics (IIAI-AAI), 2015 IIAI 4th International Congress on*, 2015, pp. 517–522.
[23] W. Wedashwara, A. H. Jatmika, I. W. A. Arimbawa, and others, "Smart solar powered hydroponics system using internet of things and fuzzy association rule mining," in *IOP Conference Series: Earth and Environmental Science*, 2021, vol. 712, no. 1, p. 12007.
[24] J. D. González-Teruel, R. Torres-Sánchez, P. J. Blaya-Ros, A. B. Toledo-Moreo, M. Jiménez-Buend\'\ia, and F. Soto-Valles, "Design and calibration of a low-cost SDI-12 soil moisture sensor," *Sensors*, vol. 19, no. 3, p. 491, 2019.
[25] W. Wedashwara, B. Irmawati, A. H. Jatmika, and A. Zubaidi, "Rancang Bangun WSN berbasis nRF24L01 dan SIM800l bertenaga Surya untuk Implementasi IoT secara Outdoor," *Edumatic: Jurnal Pendidikan Informatika*, vol. 5, no. 2, pp. 296–305, 2021.
[26] W. Wedashwara, I. W. A. Arimbawa, A. H. Jatmika, A. Zubaidi, and T. Mulyana, "IoT based Smart Small Scale Solar Energy Planning using Evolutionary Fuzzy Association Rule Mining," in *2020 International Conference on Advancement in Data Science, E-learning and Information Systems (ICADEIS)*, 2020, pp. 1–6.
[27] Y. He, Y. Tang, Y.-Q. Zhang, and R. Sunderraman, "Adaptive Fuzzy Association Rule mining for effective decision support in biomedical applications," *Int J Data Min Bioinform*, vol. 1, no. 1, pp. 3–18, 2018.
[28] X. Jiang, "Isolated Chinese sign language recognition using gray-level Co-occurrence Matrix and parameter-optimized Medium Gaussian support vector machine," in *Frontiers in Intelligent Computing: Theory and Applications*, Springer, 2020, pp. 182–193.
[29] J. Deng and Y. Deng, "Information Volume of Fuzzy Membership Function," *International Journal of Computers, Communications and Control*, vol. 16, no. 1, 2021, doi: 10.15837/ijccc.2021.1.4106.
[30] M. S. Uddin, M. Miah, M. A. A. Khan, and A. AlArjani, "Goal programming tactic for uncertain multi-objective transportation problem using fuzzy linear membership function," *Alexandria Engineering Journal*, vol. 60, no. 2, 2021, doi: 10.1016/j.aej.2020.12.039.
[31] M. Ćalasan, S. H. E. A. Aleem, and A. F. Zobaa, "On the root mean square error (RMSE) calculation for parameter estimation of photovoltaic models: A novel exact analytical solution based on Lambert W function," *Energy Convers Manag*, vol. 210, p. 112716, 2020.
[32] M. Hanif, M. Abdurohman, and A. G. Putrada, "Rice consumption prediction using linear regression method for smart rice box system," *Jurnal Teknologi dan Sistem Komputer*, vol. 8, no. 4, 2020, doi: 10.14710/jtsiskom.2020.13353.